EUROPEAN ORGANIZATION FOR NUCLEAR RESEARCH

CERN-PPE/93-33
25 February 1993

Measurement of the B^0 and B^+ lifetimes

The OPAL Collaboration

Abstract

From a data sample of approximately 240 000 hadronic Z^0 decays recorded during 1991 a sample of about 130 semileptonic B hadron decays containing a D^0, D^+ or D^{*+} has been isolated. Using silicon microvertex detector information the decay vertices in these events have been reconstructed. The average B hadron lifetime of the mix of B hadrons in this event sample is measured to be $1.51^{+0.16}_{-0.14} \pm 0.11$ ps. From the distribution of decay times in the different samples the lifetimes of the B^0 and B^+ mesons are determined to be $1.51^{+0.24+0.12}_{-0.23-0.14}$ ps and $1.51^{+0.30+0.12}_{-0.28-0.14}$ ps, respectively. The measured ratio of the B^+ to B^0 lifetimes of $1.00^{+0.33}_{-0.25} \pm 0.08$ supports expectations that the lifetimes are similar.

(Submitted to Phys. Lett.)

The OPAL Collaboration

P.D. Acton[25], G. Alexander[23], J. Allison[16], P.P. Allport[5], K.J. Anderson[9], S. Arcelli[2], A. Astbury[28], D. Axen[29], G. Azuelos[18,a], G.A. Bahan[16], J.T.M. Baines[16], A.H. Ball[17], J. Banks[16], R.J. Barlow[16], S. Barnett[16], J.R. Batley[5], G. Beaudoin[18], A. Beck[23], G.A. Beck[13], J. Becker[10], T. Behnke[27], K.W. Bell[20], G. Bella[23], P. Bentkowski[18], P. Berlich[10], S. Bethke[11], O. Biebel[3], U. Binder[10], I.J. Bloodworth[1], P. Bock[11], B. Boden[3], H.M. Bosch[11], H. Breuker[8], P. Bright-Thomas[25], R.M. Brown[20], A. Buijs[8], H.J. Burckhart[8], C. Burgard[27], P. Capiluppi[2], R.K. Carnegie[6], A.A. Carter[13], J.R. Carter[5], C.Y. Chang[17], D.G. Charlton[8], S.L. Chu[4], P.E.L. Clarke[25], I. Cohen[23], J.C. Clayton[1], W.J. Collins[5], J.E. Conboy[15], M. Cooper[22], M. Coupland[14], M. Cuffiani[2], S. Dado[22], G.M. Dallavalle[2], S. De Jong[13], L.A. del Pozo[5], H. Deng[17], A. Dieckmann[11], M. Dittmar[4], M.S. Dixit[7], E. do Couto e Silva[12], J.E. Duboscq[8], E. Duchovni[26], G. Duckeck[11], I.P. Duerdoth[16], D.J.P. Dumas[6], P.A. Elcombe[5], P.G. Estabrooks[6], E. Etzion[23], H.G. Evans[9], F. Fabbri[2], M. Fierro[2], M. Fincke-Keeler[28], H.M. Fischer[3], D.G. Fong[17], M. Foucher[17], A. Gaidot[21], O. Ganel[26], J.W. Gary[4], J. Gascon[18], R.F. McGowan[16], N.I. Geddes[20], C. Geich-Gimbel[3], S.W. Gensler[9], F.X. Gentit[21], G. Giacomelli[2], R. Giacomelli[2], V. Gibson[5], W.R. Gibson[13], J.D. Gillies[20], J. Goldberg[22], M.J. Goodrick[5], W. Gorn[4], C. Grandi[2], F.C. Grant[5], J. Hagemann[27], G.G. Hanson[12], M. Hansroul[8], C.K. Hargrove[7], P.F. Harrison[13], J. Hart[8], P.M. Hattersley[1], M. Hauschild[8], C.M. Hawkes[8], E. Heflin[4], R.J. Hemingway[6], R.D. Heuer[8], J.C. Hill[5], S.J. Hillier[8], T. Hilse[10], D.A. Hinshaw[18], J.D. Hobbs[8], P.R. Hobson[25], D. Hochman[26], R.J. Homer[1], A.K. Honma[28,a], R.E. Hughes-Jones[16], R. Humbert[10], P. Igo-Kemenes[11], H. Ihssen[11], D.C. Imrie[25], A.C. Janissen[6], A. Jawahery[17], P.W. Jeffreys[20], H. Jeremie[18], M. Jimack[2], M. Jobes[1], R.W.L. Jones[13], P. Jovanovic[1], C. Jui[4], D. Karlen[6], K. Kawagoe[24], T. Kawamoto[24], R.K. Keeler[28], R.G. Kellogg[17], B.W. Kennedy[15], S. Kluth[5], T. Kobayashi[24], D.S. Koetke[8], T.P. Kokott[3], S. Komamiya[24], L. Köpke[8], J.F. Kral[8], R. Kowalewski[6], J. von Krogh[11], J. Kroll[9], M. Kuwano[24], P. Kyberd[13], G.D. Lafferty[16], R. Lahmann[17], F. Lamarche[18], J.G. Layter[4], P. Leblanc[18], A.M. Lee[17], M.H. Lehto[15], D. Lellouch[26], C. Leroy[18], J. Letts[4], S. Levegrün[3], L. Levinson[26], S.L. Lloyd[13], F.K. Loebinger[16], J.M. Lorah[17], B. Lorazo[18], M.J. Losty[7], X.C. Lou[12], J. Ludwig[10], M. Mannelli[8], S. Marcellini[2], G. Maringer[3], C. Markus[3], A.J. Martin[13], J.P. Martin[18], T. Mashimo[24], P. Mättig[3], U. Maur[3], J. McKenna[28], T.J. McMahon[1], J.R. McNutt[25], F. Meijers[8], D. Menszner[11], F.S. Merritt[9], H. Mes[7], A. Michelini[8], R.P. Middleton[20], G. Mikenberg[26], J. Mildenberger[6], D.J. Miller[15], R. Mir[12], W. Mohr[10], C. Moisan[18], A. Montanari[2], T. Mori[24], M. Morii[24], T. Mouthuy[12,b], B. Nellen[3], H.H. Nguyen[9], M. Nozaki[24], S.W. O'Neale[1], F.G. Oakham[7], F. Odorici[2], H.O. Ogren[12], C.J. Oram[28,a], M.J. Oreglia[9], S. Orito[24], J.P. Pansart[21], B. Panzer-Steindel[8], P. Paschievici[26], G.N. Patrick[20], N. Paz-Jaoshvili[23], P. Pfister[10], J.E. Pilcher[9], J. Pinfold[31], D. Pitman[28], D.E. Plane[8], P. Poffenberger[28], B. Poli[2], A. Pouladdej[6], T.W. Pritchard[13], H. Przysiezniak[18], G. Quast[27], M.W. Redmond[9], D.L. Rees[8], G.E. Richards[16], D. Robinson[8], A. Rollnik[3], J.M. Roney[28,c], E. Ros[8], S. Rossberg[10], A.M. Rossi[2], M. Rosvick[28], P. Routenburg[6], K. Runge[10], O. Runolfsson[8], D.R. Rust[12], M. Sasaki[24], C. Sbarra[8], A.D. Schaile[10], O. Schaile[10], W. Schappert[6], P. Scharff-Hansen[8], P. Schenk[4], B. Schmitt[3], H. von der Schmitt[11], S. Schreiber[3], C. Schwick[27], J. Schwiening[3], W.G. Scott[20], M. Settles[12], T.G. Shears[5], B.C. Shen[4], C.H. Shepherd-Themistocleous[7], P. Sherwood[15], R. Shypit[29], A. Simon[3], P. Singh[13], G.P. Siroli[2], A. Skuja[17], A.M. Smith[8], T.J. Smith[28], G.A. Snow[17], R. Sobie[28,c], R.W. Springer[17], M. Sproston[20], K. Stephens[16], J. Steuerer[28], R. Ströhmer[11], D. Strom[30], T. Takeshita[24,d], P. Taras[18], S. Tarem[26], M. Tecchio[9], P. Teixeira-Dias[11], N. Tesch[3], N.J. Thackray[1], M.A. Thomson[15], E. Torrente-Lujan[22], G. Transtromer[25], N.J. Tresilian[16], T. Tsukamoto[24], M.F. Turner[8], G. Tysarczyk-Niemeyer[11], D. Van den plas[18], R. Van Kooten[27], G.J. VanDalen[4], G. Vasseur[21], C.J. Virtue[7], A. Wagner[27], D.L. Wagner[9], C. Wahl[10], J.P. Walker[1], C.P. Ward[5], D.R. Ward[5], P.M. Watkins[1], A.T. Watson[1], N.K. Watson[8], M. Weber[11], P. Weber[6], P.S. Wells[8], N. Wermes[3], M.A. Whalley[1], G.W. Wilson[4], J.A. Wilson[1], V-H. Winterer[10], T. Wlodek[26], S. Wotton[11], T.R. Wyatt[16], R. Yaari[26], A. Yeaman[13], G. Yekutieli[26], M. Yurko[18], W. Zeuner[8], G.T. Zorn[17].

[1]School of Physics and Space Research, University of Birmingham, Birmingham, B15 2TT, UK
[2]Dipartimento di Fisica dell' Università di Bologna and INFN, Bologna, 40126, Italy
[3]Physikalisches Institut, Universität Bonn, D-5300 Bonn 1, FRG
[4]Department of Physics, University of California, Riverside, CA 92521 USA
[5]Cavendish Laboratory, Cambridge, CB3 0HE, UK
[6]Carleton University, Dept of Physics, Colonel By Drive, Ottawa, Ontario K1S 5B6, Canada
[7]Centre for Research in Particle Physics, Carleton University, Ottawa, Ontario K1S 5B6, Canada
[8]CERN, European Organisation for Particle Physics, 1211 Geneva 23, Switzerland
[9]Enrico Fermi Institute and Department of Physics, University of Chicago, Chicago Illinois 60637, USA
[10]Fakultät für Physik, Albert Ludwigs Universität, D-7800 Freiburg, FRG
[11]Physikalisches Institut, Universität Heidelberg, Heidelberg, FRG
[12]Indiana University, Dept of Physics, Swain Hall West 117, Bloomington, Indiana 47405, USA
[13]Queen Mary and Westfield College, University of London, London, E1 4NS, UK
[14]Birkbeck College, London, WC1E 7HV, UK
[15]University College London, London, WC1E 6BT, UK
[16]Department of Physics, Schuster Laboratory, The University, Manchester, M13 9PL, UK
[17]Department of Physics, University of Maryland, College Park, Maryland 20742, USA
[18]Laboratoire de Physique Nucléaire, Université de Montréal, Montréal, Quebec, H3C 3J7, Canada
[20]Rutherford Appleton Laboratory, Chilton, Didcot, Oxfordshire, OX11 0QX, UK
[21]DAPNIA/SPP, Saclay, F-91191 Gif-sur-Yvette, France
[22]Department of Physics, Technion-Israel Institute of Technology, Haifa 32000, Israel
[23]Department of Physics and Astronomy, Tel Aviv University, Tel Aviv 69978, Israel
[24]International Centre for Elementary Particle Physics and Dept of Physics, University of Tokyo, Tokyo 113, and Kobe University, Kobe 657, Japan
[25]Brunel University, Uxbridge, Middlesex, UB8 3PH UK
[26]Nuclear Physics Department, Weizmann Institute of Science, Rehovot, 76100, Israel
[27]Universität Hamburg/DESY, II Inst für Experimental Physik, 2000 Hamburg 52, Germany
[28]University of Victoria, Dept of Physics, P O Box 3055, Victoria BC V8W 3P6, Canada
[29]University of British Columbia, Dept of Physics, 6224 Agriculture Road, Vancouver BC V6T 1Z1, Canada
[30]University of Oregon, Dept of Physics, Eugene, Oregon 97403, USA
[31]University of Alberta, Dept of Physics, Edmonton AB T6G 2J1, Canada

[a]Also at TRIUMF, Vancouver, Canada V6T 2A3
[b]Now at Centre de Physique des Particules de Marseille, Faculté des Sciences de Luminy, Marseille
[c]And IPP, University of Victoria, Dept of Physics, P O Box 3055, Victoria BC V8W 3P6, Canada
[d]Also at Shinshu University, Matsumoto 390, Japan

1 Introduction

The measurement of the individual lifetimes of the weakly decaying B hadrons provides a direct test of the validity of the spectator model. Variations may be expected to occur at about the 10% level [1]. Variations of this magnitude are now of significance because measurements of the average[1] B lifetime with data from the LEP experiments [2] have already reached a higher precision. Furthermore, because the average B hadron lifetimes have been used to determine the Cabibbo-Kobayashi-Maskawa matrix element governing the b quark coupling to the c quark, a large deviation from the spectator model would be important. It is therefore of interest to measure the lifetimes of the different B hadron species, which can be separated by reconstructing B hadrons in (semi-)exclusive decay modes. Using the current OPAL data, the most experimentally accessible channels for reconstructing B^0 and B^+ mesons are the semileptonic decays with a fully reconstructed charm meson, *e.g.*:

$$B \to \overline{D}^0 \ell^+ X, \qquad B \to D^- \ell^+ X, \qquad B \to D^{*-} \ell^+ X,$$

where ℓ is either an electron or a muon. Charge conjugation is implicitly assumed throughout this letter. These decay modes are expected to allow partial separation of B^+ and B^0.

In this letter we report on an analysis using precision tracking, including information provided by our silicon microvertex detector, to reconstruct the individual charm and bottom hadron decay vertices in semileptonic B decays. We calculate the decay time for each B hadron using its measured decay length and estimated energy. We use the resulting decay times to measure the exclusive B hadron lifetimes. Results are presented for the B^0 and B^+ lifetimes using our 1991 data.

2 The OPAL detector

A complete description of the OPAL detector can be found elsewhere [3, 4]. We describe briefly the aspects of the detector pertinent to this analysis. Tracking of charged particles is performed by the central detector which consists of a large volume jet chamber, a precision vertex drift chamber and chambers measuring the z-coordinate[2] of tracks as they leave the jet chamber. For the 1991 LEP run this tracking system was enhanced by the addition of a silicon microvertex detector. The central detector is positioned inside a solenoidal coil that provides a uniform magnetic field of 0.435 T. The momentum resolution obtained is approximately $(\sigma_{p_{xy}}/p_{xy})^2 = (0.02)^2 + (0.0015 p_{xy})^2$, where p_{xy} is in GeV. In addition to tracking charged particles, the jet chamber provides measurements of the ionization loss of charged particles, which are used for particle identification. The coil is surrounded by a time-of-flight counter array and a lead-glass electromagnetic calorimeter with presampler. Outside the electromagnetic calorimeter is the instrumented return yoke of the magnet, which forms the hadron calorimeter. This is surrounded by muon chambers.

Crucial to this analysis is the microvertex detector [4]. This detector consists of two concentric arrays of silicon strip detectors at radii of 6.1 cm and 7.5 cm surrounding a 5.3 cm radius beryllium beampipe. Each silicon wafer has 629 readout strips with a pitch of 50 μm. The detector has an active length of 18 cm, giving two layer acceptance for $|\cos\theta| < 0.76$.

[1] Most of the average B hadron lifetime measurements utilize inclusive semileptonic decays and therefore more closely measure a mean weighted by relative production rates and semileptonic branching fractions.

[2] The OPAL coordinate system is defined with positive z being along the electron beam direction, θ and ϕ being the polar and azimuthal angles respectively.

Within this acceptance each layer covers approximately 90% of the solid angle. The efficiency for reconstructing a hit within the fiducial region of the silicon wafers has been determined to be greater than 0.97 using $Z^0 \to \mu^+\mu^-$ decays. The detectors provide $r - \phi$ hit coordinates with an intrinsic precision better than 6 μm. However, alignment uncertainties within OPAL currently limit the space-point resolution to about 10 μm. When combined with the angle and curvature information provided by the other central detector components this results in an impact parameter resolution of 18 μm for tracks in $Z^0 \to \mu^+\mu^-$ and $Z^0 \to e^+e^-$ events.

Several simulated data samples have been used in this analysis. These samples have been generated using the JETSET program [6, 7]. For detailed studies simulated event samples were passed through a simulation of the OPAL detector [8] and were processed using the same reconstruction software as the real data. To obtain higher statistic samples, additional JETSET events were processed using a faster simulation of the OPAL detector [8]. The performance of the central detector is well described by this fast simulation.

3 Particle identification

Charged pions and kaons are identified using $\mathrm{d}E/\mathrm{d}x$ information from the jet chamber [5]. For the momentum region between 2 GeV and 20 GeV the separation between pions and kaons is greater than two standard deviations. We consider a particle to be consistent with a specific hypothesis if the probability for the measured $\mathrm{d}E/\mathrm{d}x$ value is calculated to be greater than 1%. For kaons, if the measured $\mathrm{d}E/\mathrm{d}x$ is higher than the expected value, we tighten this requirement to 3%.

The electron identification procedure used in this analysis is the same as that described in a previous publication [9] and covers the angular range $|\cos\theta| < 0.70$. It uses the $\mathrm{d}E/\mathrm{d}x$ measured in the jet chamber, shower shape information from the electromagnetic calorimeter and presampler, and the quantity E_{cone}/p, where E_{cone} is the energy deposited in the calorimeter in a cone around the extrapolated position of the central detector track of momentum p. Furthermore, electron candidates which are identified as arising from photon conversions are rejected. In the kinematic range relevant to this analysis the electron identification efficiency is about 55%. The probability to misidentify a hadron as an electron is of the order of 0.1%.

Muons are identified by associating central detector tracks with track segments in the muon chambers, requiring a position match in two orthogonal coordinates. In addition, loose requirements on $\mathrm{d}E/\mathrm{d}x$ are made to reject kaons and protons. The average identification efficiency is approximately 75% for muons with $p > 3$ GeV and $|\cos\theta| < 0.90$. Hadrons may fake muons either by being misidentified or by decaying in flight to muons. The average probability for a hadron to fake a prompt muon in this kinematic range is estimated to be 0.7%.

4 Event selection

This analysis is based on about 11.1 pb^{-1} of data recorded in 1991 after the microvertex detector was commissioned. The data were collected from e^+e^- annihilations at centre of mass energies between 88.5 and 93.8 GeV. The selection criteria for hadronic Z^0 decays are described elsewhere [10]. The efficiency of the hadronic selection criteria is determined to be $(98.4 \pm 0.4)\%$. After data quality and detector performance requirements, the available data sample consists of about 240 000 events.

Decay mode	$E_{\mathrm{D}^{(*)}}$ (GeV)	p_{K} (GeV)	p_{π} (GeV)	$\mid \cos\theta^{*} \mid$	$m_{\mathrm{D}^{(*)}\ell}$ (GeV)	$E_{\mathrm{D}^{(*)}\ell}$ (GeV)	$l_{\mathrm{D}}/\sigma_{l}$
$\mathrm{D}^{0} \to \mathrm{K}^{-}\pi^{+}$	> 6	> 2	> 1	< 0.8	> 3.0	> 13.5	> -1
$\mathrm{D}^{+} \to \mathrm{K}^{-}\pi^{+}\pi^{+}$	> 9	> 2	> 0.8	< 0.8	> 3.2	> 13.5	> -1
$\mathrm{D}^{*+} \to \mathrm{D}^{0}\pi^{+}$, $\mathrm{D}^{0} \to \mathrm{K}^{-}\pi^{+}$	> 5	> 0.15	> 0.15	< 0.95	> 2.8	> 9.0	-
$\mathrm{D}^{*+} \to \mathrm{D}^{0}\pi^{+}$, $\mathrm{D}^{0} \to \mathrm{K}^{-}\pi^{+}\pi^{+}\pi^{-}$	> 9	> 2	> 0.5	-	> 3.0	> 13.5	-

Table 1: Decay mode dependent selection criteria.

The selection of $\mathrm{B} \to \overline{\mathrm{D}}\ell^{+}\mathrm{X}$ and $\mathrm{B} \to \overline{\mathrm{D}}^{*}\ell^{+}\mathrm{X}$ events uses both kinematic and vertex information of the decays. In table 1 we summarize the selection criteria for the four different decay modes which we consider. The kinematic selection is similar to that used in a previous OPAL analyse [11]. D mesons are selected by considering all track combinations consistent with the appropriate particle identification hypotheses. To reduce combinatorial background D and D* meson candidates are required to have energy ($E_{\mathrm{D}^{(*)}}$) greater than 5–9 GeV depending on the decay mode. We use the symbol $\mathrm{D}^{(*)}$ to denote either a D or D* meson. To select D^{*+} candidates we require a π^{+} in addition to a D^{0} candidate. The difference between the mass of the D^{*+} candidate and that of the D^{0} is required to be in the range 0.142–0.148 GeV. To further reduce the background we require the momenta of the decay products (p_{K} and p_{π}) to satisfy minimum momentum criteria. For some decay modes we also cut on $\cos\theta^{*}$, where θ^{*} is the angle between the K^{-} and the D boost direction in the D rest frame. For the D^{+} candidates we also require that the mass of each $\mathrm{K}^{-}\pi^{+}$ combination be less than 1.55 GeV. This cut rejects partially reconstructed D^{0} decays which form a peak at about 1.6 GeV and could fake a D^{+} if combined with a pion from a $\mathrm{D}^{*+} \to \mathrm{D}^{0}\pi^{+}$ decay, but provides high efficiency for D^{+} decays because they are predominantly three-body [12].

Lepton candidates are required to have $p > 2$ GeV. All $\overline{\mathrm{D}}^{(*)}\ell^{+}$ combinations are considered as possible B candidates. To suppress random combinations we require the mass ($m_{\mathrm{D}^{(*)}\ell}$) and energy ($E_{\mathrm{D}^{(*)}\ell}$) of the candidates to satisfy certain minimum criteria. In addition all candidates are required to have $m_{\mathrm{D}^{(*)}\ell} < 5.35$ GeV.

In order to reject poorly determined and possibly badly reconstructed decays we require that the lepton track and at least two of the D decay tracks each be associated with at least one hit in the microvertex detector. This ensures that vertex reconstruction is dominated by tracks with microvertex detector information. The association of microvertex hits to tracks found in the other central tracking components requires that the probability associated with the χ^{2} be greater than 0.1% for all matches. Using a simulation of the OPAL detector [8] we find that particles leaving two (one) hits in the microvertex detector and resulting in a reconstructed track in the central detector have these hits correctly associated 96% (93%) of the time and

Decay mode	Number of candidates	Estimated Background	Signal
$D^0 \to K^-\pi^+$	82	23	59 ± 9
$D^+ \to K^-\pi^+\pi^+$	62	20	42 ± 8
$D^{*+} \to D^0\pi^+$, $D^0 \to K^-\pi^+$	28	5	23 ± 5
$D^{*+} \to D^0\pi^+$, $D^0 \to K^-\pi^+\pi^+\pi^-$	20	7	13 ± 4

Table 2: Number of events and background for each decay mode.

are matched with one or more incorrect hits 2% (5%) of the time.

To reconstruct the decay vertices we minimize the χ^2 for a vertex fit with respect to $(x_B, y_B, l_D, \kappa_1 \ldots \kappa_i, \phi_1 \ldots \phi_i)$, where (x_B, y_B) are the coordinates of the B decay vertex, l_D is the decay length of the D meson and κ_i and ϕ_i are the curvature and angle of the i^{th} track at the relevant decay vertex. The direction of flight of the D meson is fixed to correspond to its momentum vector. We demand that the probability for the vertex fit be greater than 1% in order to suppress random track combinations and badly reconstructed vertices. The B hadron decay length is calculated in the $r - \phi$ plane using the position of the reconstructed $\overline{\mathrm{D}}^{(*)}\ell^+$ vertex and the average e^+e^- interaction point. The B decay length is signed according to the cosine of the angle between the vector separating (x_B, y_B) from the average interaction point and the $\overline{\mathrm{D}}^{(*)}\ell^+$ momentum vector. To convert the decay length into three dimensions we estimate $\sin\theta$ for the B hadron from the $\overline{\mathrm{D}}^{(*)}\ell^+$ momentum vector. The B hadrons have typical decay lengths of 3 mm which are reconstructed with a resolution of about 300 μm. We require the error on the B decay length to be less than 5 mm to reject a small fraction of poorly measured decays. The D^0 (D^+) mesons have typical decay lengths of 1 mm (2.5 mm) and the typical decay length resolution is about 800 μm. As the reconstructed D decay length (l_{D}) is independent of the B hadron production point and therefore also of the B hadron decay length, we can use this to reject background. For all decay modes we require $|l_{\mathrm{D}}| < 1$ cm. For the inclusive D^0 and D^+ samples we require a decay length significance ($l_{\mathrm{D}}/\sigma_l > -1$), where σ_l is the resolution on l_{D}.

The resulting signals for the four different decay modes together with the corresponding $\overline{\mathrm{D}}^{(*)}\ell^-$ combinations are shown in figures 1 and 2. A clear signal is visible in each of these decay modes. The $K^-\pi^+$ mass distributions also show indications of a peak around 1.6 GeV. An enhancement is expected in this region from the decays $D^0 \to K^-\pi^+\pi^0$, in which the π^0 is not reconstructed. A similar, but broader, enhancement is seen in the $K^-\pi^+\pi^+$ mass distribution. Our simulation indicates that we should expect appreciable contributions from the decays $D^0 \to K^-\pi^+\pi^+\pi^-$ and $D^+ \to K^-\pi^+\pi^+\pi^0$. We have determined the signal and background in each channel by fitting the mass distributions using a function consisting of a sum of Gaussians and a second order polynomial background term. The widths of the signal Gaussians are determined from a full simulation of the OPAL detector [8]. The enhancements

around 1.6 GeV are also parameterized as Gaussians and included in the fit. The background levels in the signal regions are found to be insensitive to this parameterization. The $\overline{\mathrm{D}}^{(*)}\ell^-$ combinations provide a direct measure of the possible background of D mesons combined with fake leptons. No significant signals are observed in the $\overline{\mathrm{D}}^{(*)}\ell^-$ combinations and for each decay mode the number of $\overline{\mathrm{D}}^{(*)}\ell^-$ combinations within the signal mass regions are consistent with the combinatorial background levels under the D mass peaks in the $\overline{\mathrm{D}}^{(*)}\ell^+$ combinations. We therefore conclude that the possible background from this source is negligible.

For the lifetime determinations we select candidates in the mass range ± 60 MeV around the nominal D meson masses [12]. In order to have statistically independent samples for the lifetime analysis we remove 14 events from the $\mathrm{D}^0 \to \mathrm{K}^-\pi^+$ sample which are also identified as D^{*+} candidates. The resulting signals and estimated backgrounds are listed in table 2.

5 Lifetime fitting

In order to convert the measured decay lengths into decay times it is necessary to estimate the energy of the B hadrons. We do this by using the kinematics of the B hadron decays to correct for the missing energy on an event-by-event basis. This method effectively eliminates any dependence of the decay time distribution on the b quark fragmentation function. In order to estimate the B hadron energy (E) from the observed decay products we use the following estimator:

$$E = \frac{E_{\mathrm{D}^{(*)}\ell} \cdot m_{\mathrm{B}}}{m_{\mathrm{D}^{(*)}\ell}}(1 + a_1\Delta m + a_2\Delta m^2), \tag{1}$$

where $\Delta m = (m_{\mathrm{B}} - m_{\mathrm{D}^{(*)}\ell})/m_{\mathrm{B}}$ for $m_{\mathrm{D}^{(*)}\ell} < m_{\mathrm{B}}$ and $\Delta m = 0$ for $m_{\mathrm{D}^{(*)}\ell} > m_B$. The parameters a_1 and a_2 may depend on the decay mode and any selection criteria applied. We have determined these parameters individually, for each decay mode of interest, using simulated event samples selected with the same criteria as used for the data. The parameters were found to be similar for all the decay modes. For example, for the $\mathrm{B} \to \overline{\mathrm{D}}^0\ell^+\mathrm{X}$ decays we find $a_1 = 0.02$ and $a_2 = -0.80$. Our simulation shows that this method of correcting for the missing energy is independent of the B energy spectrum and hence of uncertainties in the fragmentation function.

In addition to the B energy, we also estimate its uncertainty on an event-by-event basis. The width of the energy resolution function has a strong dependence on the visible mass ($m_{\mathrm{D}^{(*)}\ell}$). We use the form:

$$\sigma_E/E = b_0 + b_1\Delta m. \tag{2}$$

We determine the parameters b_0 and b_1 using our simulation. Typical values are $b_0 = 0.025$ and $b_1 = 0.40$ corresponding to $\sigma_E/E \sim 8\%$ for $m_{\mathrm{D}^{(*)}\ell} = 4.5$ GeV and $\sigma_E/E \sim 21\%$ for $m_{\mathrm{D}^{(*)}\ell} = 3$ GeV.

Using the individual decay length and energy estimates we calculate the decay time (t_i) for each $\mathrm{B} \to \overline{\mathrm{D}}^{(*)}\ell^+\mathrm{X}$ candidate and use an unbinned maximum likelihood fit to extract the B hadron lifetimes. The B decay time distribution ($\mathcal{F}_{\mathrm{B}}$) is expected to be an exponential convolved with Gaussian resolution functions. For each candidate the resolution on the decay time (σ_{t_i}) is given by:

$$\frac{\sigma_{t_i}^2}{t_i^2} = \frac{\sigma_{l_i}^2}{l_i^2} + \frac{\sigma_{E_i}^2}{E_i^2}, \tag{3}$$

Decay mode	Fitted lifetime (ps)
$D^0 \to K^-\pi^+$	$1.54^{+0.25}_{-0.21}$
$D^+ \to K^-\pi^+\pi^+$	$1.30^{+0.27}_{-0.22}$
$D^{*+} \to D^0\pi^+$, $D^0 \to K^-\pi^+$	$1.71^{+0.45}_{-0.34}$
$D^{*+} \to D^0\pi^+$, $D^0 \to K^-\pi^+\pi^+\pi^-$	$1.67^{+0.61}_{-0.42}$
Combined D^{*+}	$1.70^{+0.35}_{-0.27}$
Combined sample	$1.51^{+0.16}_{-0.14}$

Table 3: Lifetime fit results for different $\overline{D}^{(*)}\ell^+$ samples.

where σ_{l_i} is the error on the decay length. The decay time resolution receives roughly equal contributions from each source.

To take into account the background when fitting for the lifetimes we have studied samples selected outside the signal regions and in the $\overline{D}^{(*)}\ell^-$ events. Our simulation indicates that these event samples provide a good description of the apparent decay time distribution of the background events. We find that in all cases the apparent lifetime distribution of these samples is almost symmetric about zero. This is also found to be the case for the simulated background events. Consequently we have parameterized the background lifetime distributions as the sum of two Gaussians:

$$\mathcal{F}_{back} = \frac{1-c_1}{\sigma_i\sqrt{2\pi}}\exp(\frac{-{t_i}^2}{2{\sigma_i}^2}) + \frac{c_1}{\sqrt{{\sigma_i}^2+{c_2}^2}\sqrt{2\pi}}\exp(\frac{-(t_i-c_3)^2}{2({\sigma_i}^2+{c_2}^2)}), \tag{4}$$

where $\sigma_i = \sigma_{l_i} \cdot t_i/l_i$ is the expected measurement resolution. The parameters c_1, c_2 and c_3 determine the fraction of events described by the second Gaussian and its mean and width. These are determined by fitting the data samples. All the fits give consistent results and indicate that about half of the background is described by the first Gaussian in equation 4, corresponding to the resolution function. The remainder is described by a broad Gaussian of width $\sim$ 2 ps. This contribution represents the various random combinations of B tracks combined with unrelated tracks. Since the different background samples yield similar results we use a fit to a combined sample to describe the background in all channels. This fit results in $c_1 = 0.46 \pm 0.05$, $c_2 = 2.02 \pm 0.18$ ps and $c_3 = 0.34 \pm 0.21$ ps. The result of this maximum likelihood fit is shown in figure 3. The sensitivity of our results to the assumed shape of the background is discussed in section 7.

In order to determine the lifetime from each of the samples we use a likelihood function of the form:

$$\mathcal{F} = f \cdot \mathcal{F}_{\rm B} + (1-f) \cdot \mathcal{F}_{back}, \tag{5}$$

where the signal fractions (f) are as determined in section 4 (see table 2).

Figure 4 shows the resulting fits to the data for the three different decay modes that we have considered. The resulting lifetimes are summarized in table 3. The errors shown are statistical

only. All the lifetime measurements are consistent with each other. The average B hadron lifetime determined from the combined sample is $\langle\tau\rangle = 1.51^{+0.16}_{-0.14}$ ps.

6 Determination of the B^0 and B^+ lifetimes

The different samples of $\overline{D}^{(*)}\ell^+$ events are expected to contain different fractions of B^0 and B^+ decays. The primary sources of these events are expected to be the semileptonic decays of B^0 and B^+ mesons to pseudo-scalar, vector and p-wave charmed mesons (the so-called D^{**}'s):

$$\begin{array}{lll} B^0 \to D^-\ell^+\nu, & B^0 \to D^{*-}\ell^+\nu, & B^0 \to D^{**-}\ell^+\nu, \\ B^+ \to \overline{D}^0\ell^+\nu, & B^+ \to \overline{D}^{*0}\ell^+\nu, & B^+ \to \overline{D}^{**0}\ell^+\nu. \end{array}$$

We use the symbol D^{**} to represent, in addition to the p-wave states, possible non-resonant decays of the type $B \to \overline{D}(n\pi)\ell^+X$ and higher spin states. Decays of the B_s and B baryons to final states containing a $\overline{D}^{(*)}\ell^+$ combination *e.g.* $B_s \to D^*_{s1}(2536)^-\ell^+\nu$, $D^*_{s1}(2536)^- \to D^*\overline{K}^0$, are expected to form less than 5% of the event sample. This source of events is expected to be negligible unless the lifetimes of the B_s or B baryons differ significantly from those of the B^0 and B^+. The first measurements of the B_s and B baryon lifetimes [13] indicate that they are close to the average. Combinations of $\overline{D}^{(*)}\ell^+$ may also result from B meson decays of the type $B \to D_s^{(*)+}\overline{D}^{(*)}$, $D_s^{(*)+} \to \ell^+X$. Using the branching ratio $B(B \to D_s^{(*)+}\overline{D}^{(*)}) = 6.5 \pm 1.9\%$ [12], we estimate that the fraction of the $\overline{D}^{(*)}\ell^+$ event samples from this source is in the range 0.6–1.5%. These decays are therefore completely negligible within the current statistics.

In the absence of any D^{**} production the states containing a $D^-\ell^+$ and $D^{*-}\ell^+$ would be almost completely B^0 since D^{*0} decays always result in D^0. With the addition of D^{**} production B^+ may also decay to these combinations. Consequently the relative fraction of B^0 and B^+ mesons in the different $\overline{D}^{(*)}\ell^+$ samples depends on the relative production rate of the B mesons, their lifetimes (τ^0 and τ^+), the fractions (f^0, f^* and f^{**}) of semileptonic decays resulting in a D, D^* or D^{**} and the decay modes of the different D^* and D^{**} mesons.

We assume that the production rates of the B^0 and B^+ mesons in Z^0 decays are equal. This is expected because of isospin symmetry and the small mass difference between the states [12]. The sample compositions depend on the relative lifetimes because the partial widths for semileptonic B meson decays are dominated by spectator processes. Consequently the semileptonic branching ratios are expected to be proportional to the lifetimes.

Experimentally little is known about the production rates of the different possible D^{**} states in semileptonic B decays. The decays of the D^{**} states may result in both pseudo-scalar and vector charmed mesons and it is the relative importance of these decays which determines the compositions of the $\overline{D}^{(*)}\ell^+$ samples. We parameterize these uncertainties in terms of:

$$p_v = \frac{B(D^{**} \to D^*X)}{B(D^{**} \to D^*X) + B(D^{**} \to DX)}. \tag{6}$$

In addition we assume that the D^{**} decays are dominated by the modes $D^{**} \to D^{(*)}\pi$ and use isospin to determine the relative fraction of the decays yielding charged and neutral $D^{(*)}$'s:

$$\begin{aligned} B(D^{**+} \to D^{(*)0}\pi^+) &= 2B(D^{**+} \to D^{(*)+}\pi^0), \\ B(D^{**0} \to D^{(*)+}\pi^-) &= 2B(D^{**0} \to D^{(*)0}\pi^0). \end{aligned} \tag{7}$$

With these assumptions the relative fractions ($\mathcal{R}$) of B^0 and B^+ mesons in the different $\overline{D}^{(*)}\ell^+$ samples may be expressed as follows:

$$\mathcal{R}\left(\frac{B^0 \to \overline{D}^0\ell^+X}{B^+ \to \overline{D}^0\ell^+X}\right) = \frac{\tau^0}{\tau^+}\left(\frac{(1-\eta^*)b^0 f^* + \frac{2}{3}f^{**} + \frac{1}{3}(1-\eta^*)b^0 p_v f^{**}}{f^0 + f^* + \frac{1}{3}f^{**} + \frac{2}{3}(1-\eta^*)b^0 p_v f^{**}}\right),$$

$$\mathcal{R}\left(\frac{B^0 \to D^-\ell^+X}{B^+ \to D^-\ell^+X}\right) = \frac{\tau^0}{\tau^+}\left(\frac{f^0 + (1-b^0)f^* + \frac{1}{3}(1-p_v)f^{**} + \frac{1}{3}(1-b^0)p_v f^{**}}{\frac{2}{3}(1-b^0)p_v f^{**} + \frac{2}{3}(1-p_v)f^{**}}\right), \quad (8)$$

$$\mathcal{R}\left(\frac{B^0 \to D^{*-}\ell^+X}{B^+ \to D^{*-}\ell^+X}\right) = \frac{\tau^0}{\tau^+}\left(\frac{f^* + \frac{1}{3}p_v f^{**}}{\frac{2}{3}p_v f^{**}}\right).$$

Here b^0 is the branching ratio $B(D^{*+} \to D^0\pi^+)$, and η^* is the relative efficiency for reconstruction a D^{*+}, after reconstructing a D^0. We use the recent CLEO [14] measurement of $b^0 = 0.68 \pm 0.03$ and using our simulation determine $\eta^* = 0.76 \pm 0.03$. The uncertainties on f^{**} and p_v completely dominate the uncertainties in the composition of the samples, so we only need to consider variations in these parameters.

In order to determine f^0, f^* and f^{**} we use measurements of the inclusive and exclusive semileptonic branching ratios of the B^0 or B^+ determined at the $\Upsilon(4S)$ [15, 16, 17]. The average exclusive branching ratios [12] for B decays to $D\ell^+\nu$ and $D^*\ell^+\nu$ are consistent for the B^0 or B^+. We therefore average over charged and neutral states and combine these numbers with the CLEO [16] measurement of $f^{**} = 0.36 \pm 0.12$ to obtain:

$$f^0 = \frac{B(B \to \overline{D}\ell^+\nu)}{B(B \to \overline{D}\ell^+\nu) + B(B \to \overline{D}^*\ell^+\nu)}(1 - f^{**}) = 0.17,$$

$$f^* = \frac{B(B \to \overline{D}^*\ell^+\nu)}{B(B \to \overline{D}\ell^+\nu) + B(B \to \overline{D}^*\ell^+\nu)}(1 - f^{**}) = 0.47.$$

The fractions of B^0 and B^+ in the event samples are insensitive to the ratio f^0/f^* so only variations in f^{**} are considered when evaluating the uncertainty in the sample compositions. In equation 6 we have implicitly assumed that the reconstruction efficiencies for a particular $B \to \overline{D}^{(*)}\ell^+X$ decay are independent of the exclusive B decay mode. The corrections due to the differences in the relative efficiencies are small. Using our simulation we find them to be in the range 0.94–1.00 for the $B \to \overline{D}^*\ell^+\nu$ decays and in the range 0.77–0.95 for the $B \to \overline{D}^{**}\ell^+\nu$ decays. Figure 5a shows the variation of the fraction of B^0 in the different $\overline{D}^{(*)}\ell^+$ samples as a function of f^{**}, after applying these corrections.

In order to estimate the remaining unknown p_v one needs to estimate the relative production rates and branching fractions of the different p-wave states. Estimates of p_v are not particularly sensitive to any reasonable assumptions about the production rates. We combine the predictions of the relative production rates from [18] with predictions [19] and measurements [12] of the branching ratios to obtain $p_v = 0.54$. This value is consistent with the ARGUS data [17] which suggest that a significant fraction of the neutral D^{**}'s are the $J^P = 1^+$ and 2^+ states $D_1(2420)^0$ and $D_2^*(2460)^0$ respectively. In figure 5b we show the variation of the fractions of B^0 in the samples as function of p_v. We have taken $p_v = 0.54$, but allow a large variation of ± 0.3 when considering uncertainties in the sample compositions to allow for all reasonable variations in the decay modelling.

In order to fit for τ^0 and τ^+ we carry out a maximum likelihood fit to the combined sample of $\overline{\mathrm{D}}^{(*)}\ell^+$ events. The likelihood function ($\mathcal{F}_\mathrm{B}$) given in equation 5 is modified to become the sum of two exponentials convolved with Gaussians where the relative weight is determined by the assigned probability of a particular event being B^0 or B^+, according to equation 8. We have carried out a simulation to verify that we are able to determine the different individual lifetimes from a combined fit. A Monte Carlo sample was generated with $\tau^0 = 1.2$ ps and $\tau^+ = 1.6$ ps. The B decays were modelled with $f^{**} = 0.36$ and $p_v = 0.54$. The maximum likelihood fit yields $\tau^0 = 1.169 \pm 0.046$ ps and $\tau^+ = 1.541 \pm 0.036$ ps in agreement with the generated values. The incomplete separation between the B^0 and B^+ mesons in the $\overline{\mathrm{D}}^{(*)}\ell^+$ samples results in a significant increase in the statistical error because of correlations between the lifetime functions.

We have carried out a maximum likelihood fit to the complete $\overline{\mathrm{D}}^{(*)}\ell^+$ data sample, as shown in figure 6. The fit result is:

$$\tau^0 = 1.51^{+0.24}_{-0.23} \text{ ps},$$

$$\tau^+ = 1.51^{+0.30}_{-0.28} \text{ ps}.$$

We have also fitted directly the lifetime ratio and obtain $\tau^+/\tau^0 = 1.00^{+0.33}_{-0.25}$.

7 Systematic uncertainties

In order to evaluate the uncertainties in the sample compositions we allow f^{**} to vary by ± 0.12 and p_v to vary by ± 0.30. These variations have been conservatively chosen to cover all reasonable values for these parameters.

To estimate the uncertainties due to the background fractions and the apparent background lifetimes we have varied the parameters c_1 and c_3 (see equation 4) which determine the decay time distribution, by $\pm 2\sigma$. This variation was chosen to allow for possible differences between the different samples. To investigate further the sensitivity of the fit results to the shape of the background apparent decay time distribution we have considered a different parameterization including an exponential term. The resulting changes to the B^0 and B^+ lifetimes were negligible. We have also varied the total background fractions in each of the samples independently by $\pm 1\sigma$. Finally we have considered the extreme case of changing the background fractions in all samples by $\pm 1\sigma$ simultaneously.

We have investigated possible biases in the energy estimator (equation 1) by looking separately at Monte Carlo samples of D, D^* and D^{**} decays. The maximum deviation from unity is 2.7% which we consider as a possible systematic uncertainty. The energy resolution is well described by a Gaussian at the 10% level. However, we consider 20% variations in its value.

We have also considered possible detector effects. To allow for uncertainties in the detector resolutions we have considered variations of $\pm 20\%$ in the decay length resolutions. As a further check we have repeated the maximum likelihood fit with a fitted global error scale factor (k) multiplying the σ_{l_i} in equation 3. The fit yields $\tau^0 = 1.50 \pm 0.24$ ps, $\tau^+ = 1.50^{+0.30}_{-0.28}$ ps and $k = 1.08 \pm 0.28$, indicating that our tracking errors are well understood. We have also considered the effects of possible systematic biases in the track reconstruction due to misalignment of the microvertex detector. Because of the limited statistics of the B decay sample we have studied three charged track decay vertices in τ decays. The effect of coherent radial shifts of the microvertex detector by ± 50 μm together with incoherent shifts of ± 100 μm was found to

Systematic source	τ^0 (ps)	τ^+ (ps)	τ^+/τ^0	$\langle\tau\rangle$ (ps)
f^{**} ± 0.12	± 0.01	± 0.01	± 0.01	-
p_v ± 0.30	± 0.02	± 0.03	± 0.03	-
Background	$^{+0.04}_{-0.09}$	$^{+0.05}_{-0.08}$	$^{+0.05}_{-0.06}$	$^{+0.05}_{-0.06}$
Energy Estimator	± 0.04	± 0.04	-	± 0.04
σ_E $\pm 20\%$	± 0.03	± 0.03	-	± 0.03
σ_l $\pm 20\%$	$^{+0.04}_{-0.03}$	$^{+0.04}_{-0.03}$	-	$^{+0.04}_{-0.03}$
microvertex alignment	± 0.07	± 0.07	-	± 0.07
Interaction point	± 0.01	± 0.01	-	± 0.01
Fit method	± 0.05	± 0.05	± 0.05	± 0.02
Total	$^{+0.12}_{-0.14}$	$^{+0.12}_{-0.14}$	± 0.08	± 0.11

Table 4: Summary of systematic errors.

translate into a decay length error of ± 43 μm. We have conservatively assumed that any such effects might scale directly with the mass of the decaying particle because of the larger track opening angle and therefore consider a variation of ± 130 μm. Possible effects due to variations in the size and position of the e^+e^- interaction point have been studied by considering variations of ± 25 μm in both the x and y directions using simulated decays and are estimated to be less than 0.01 ps.

In simulated events the vertex reconstruction and lifetime fit methods have been shown to reproduce the average B hadron lifetime at the level of 0.02 ps and the individual B^0 and B^+ lifetimes at the level of 0.05 ps. We assign these numbers as additional systematic errors in the method.

The resulting systematic uncertainties are summarized in table 4. We have combined all systematic errors in quadrature.

8 Conclusions

We have used a sample of about 130 (semi-)exclusive $B \to \overline{D}\ell^+X$ and $B \to \overline{D}^*\ell^+X$ decays to directly measure the B^0 and B^+ lifetimes. We find:

$$\tau^0 = 1.51^{+0.24+0.12}_{-0.23-0.14} \text{ ps},$$

$$\tau^+ = 1.51^{+0.30+0.12}_{-0.28-0.14} \text{ ps},$$

$$\tau^+/\tau^0 = 1.00^{+0.33}_{-0.25} \pm 0.08.$$

Our results confirm indirect results [12], obtained by the ARGUS and CLEO collaborations, that the B^0 and B^+ lifetimes are similar. The measured average B lifetime for the mix of B hadrons in this event sample is $\langle\tau\rangle = 1.51^{+0.16}_{-0.14} \pm 0.11$ ps, in good agreement with less direct measurements using inclusive leptons [2]. These measurements are also in agreement with similar results obtained by the DELPHI collaboration [20].

Acknowledgements

It is a pleasure to thank the SL Division for the efficient operation of the LEP accelerator, the precise information on the absolute energy, and their continuing close cooperation with our experimental group. In addition to the support staff at our own institutions we are pleased to acknowledge the
Department of Energy, USA,
National Science Foundation, USA,
Texas National Research Laboratory Commission, USA,
Science and Engineering Research Council, UK,
Natural Sciences and Engineering Research Council, Canada,
Fussefeld Foundation,
Israeli Ministry of Energy,
Israeli Ministry of Science,
Minerva Gesellschaft,
Japanese Ministry of Education, Science and Culture (the Monbusho) and a grant under the Monbusho International Science Research Program,
German Israeli Bi-national Science Foundation (GIF),
Direction des Sciences de la Matière du Commissariat à l'Energie Atomique, France,
Bundesministerium für Forschung und Technologie, FRG,
National Research Council of Canada, Canada,
A.P. Sloan Foundation and Junta Nacional de Investigação Científica e Tecnológica, Portugal.

References

[1] J. H. Kühn *et al.*, in 'Z physics at LEP 1', *CERN 89-08* (1989) ed. G. Altarelli *et al.*

[2] ALEPH Collaboration, D. Buskulic *et al.*, *CERN-PPE/92-133* (1992);
DELPHI Collaboration, P. Abreu *et al.*, *Z. Phys.* **C53** (1992) 567;
L3 Collaboration, B. Adeva *et al.*, *Phys. Lett.* **B270** (1992) 111;
OPAL Collaboration, P. D. Acton *et al.*, *Phys. Lett.* **B274** (1992) 513.

[3] OPAL Collaboration, K. Ahmet *et al.*, *Nucl. Instrum. Methods* **A305** (1991) 275.

[4] P. P. Allport *et al.*, *Nucl. Instrum. Methods* **A324** (1993) 34.

[5] M. Hauschild *et al.*, *Nucl. Instrum. Methods* **A314** (1992) 74.

[6] T. Sjöstrand, *Comp. Phys. Comm.* **39** (1986) 347.

[7] OPAL Collaboration, M. Z. Akrawy *et al.*, *Z. Phys.* **C47** (1990) 505.

[8] J. Allison *et al.*, *Nucl. Instrum. Methods* **A317** (1992) 47.

[9] OPAL Collaboration, P. D. Acton *et al.*, *Phys. Lett.* **B276** (1992) 379. More details can be found in: OPAL Collaboration, P. D. Acton *et al.*, *Z. Phys.* **C55** (1992) 191.

[10] OPAL Collaboration, G. Alexander *et al.*, *Z. Phys.* **C52** (1991) 175.

[11] OPAL Collaboration, P. D. Acton *et al.*, *Phys. Lett.* **B295** (1992) 357.

[12] Particle Data Group, K. Hikasa *et al.*, *Phys. Rev.* **D45** (1992) 1.

[13] ALEPH Collaboration, D. Buskulic *et al.*, *CERN-PPE/92-138* (1992);
DELPHI Collaboration, P. Abreu *et al.*, *Phys. Lett.* **B289** (1992) 199.

[14] CLEO Collaboration, F. Butler *et al.*, *CLNS 92-1143* (1992).

[15] ARGUS Collaboration, H. Albrecht *et al.*, *Phys. Lett.* **B197** (1987) 452;
ARGUS Collaboration, H. Albrecht *et al.*, *Phys. Lett.* **B229** (1989) 175;
ARGUS Collaboration, H. Albrecht *et al.*, *Phys. Lett.* **B275** (1992) 195;
CLEO Collaboration, D. Bortoletto *et al.*, *Phys. Rev. Lett.* **63** (1989) 1667.

[16] CLEO Collaboration, R. Fulton *et al.*, *Phys. Rev.* **D43** (1991) 651.

[17] ARGUS Collaboration, H. Albrecht *et al.*, *DESY 92-146* (1992).

[18] P. Colangelo, G. Nardulli and N. Paver, *Phys. Lett.* **B293** (1992) 207.

[19] J. L. Rosner, *Comm. Nucl. Part. Phys.* (1986) 109;
S. Godfrey and R. Kokoski, *Phys. Rev.* **D43** (1991) 1679.

[20] DELPHI Collaboration, P. Abreu *et al.*, *CERN-PPE/92-174* (1992), submitted to *Z. Phys.*

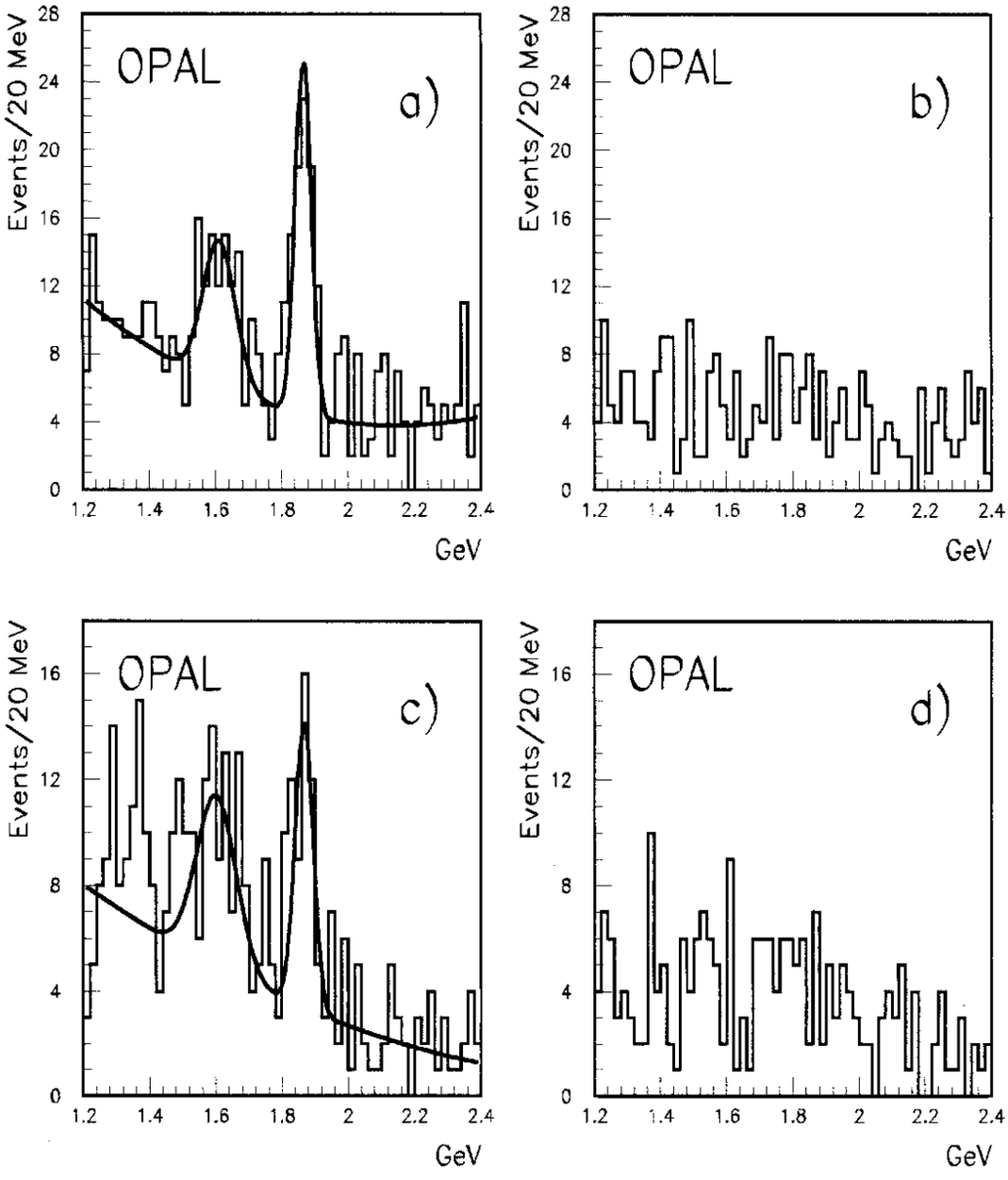

Figure 1: (a) Mass distribution of $K^-\pi^+$ combinations for events containing an ℓ^-. (b) Mass distribution of $K^-\pi^+$ combinations for events containing an ℓ^+. (c) Mass distribution of $K^-\pi^+\pi^+$ combinations for events containing an ℓ^-. (d) Mass distribution of $K^-\pi^+\pi^+$ combinations for events containing an ℓ^+. The curves shown are the results of fits using Gaussians plus polynomial background functions.

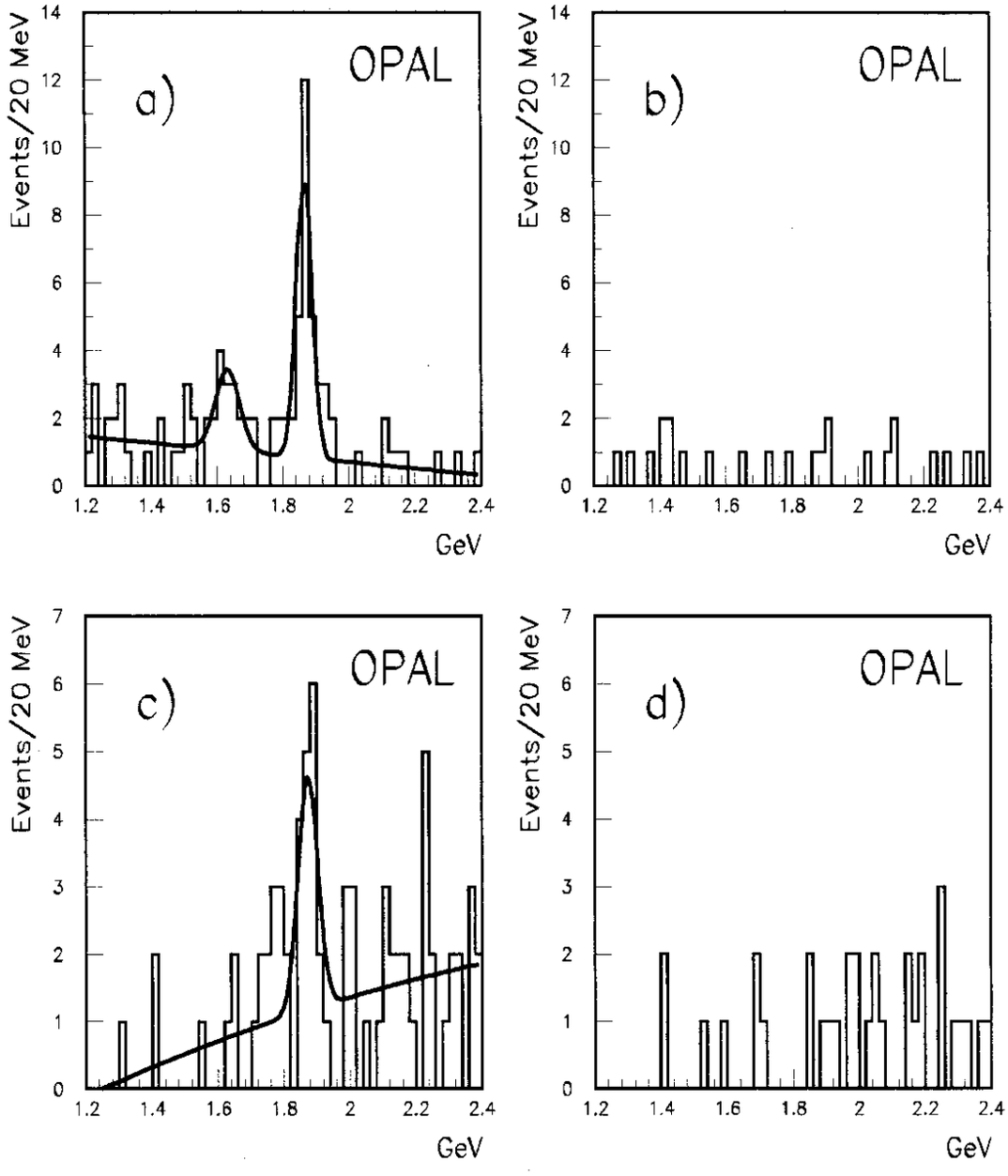

Figure 2: Mass distributions for events satisfying the D^{*+} selection cut. (a) Mass distribution of $K^-\pi^+$ combinations for events containing an ℓ^-. (b) Mass distribution of $K^-\pi^+$ combinations for events containing an ℓ^+. (c) Mass distribution of $K^-\pi^+\pi^+\pi^-$ combinations for events containing an ℓ^-. (d) Mass distribution of $K^-\pi^+\pi^+\pi^-$ combinations for events containing an ℓ^+. The curves shown are the results of fits using Gaussians plus polynomial background functions.

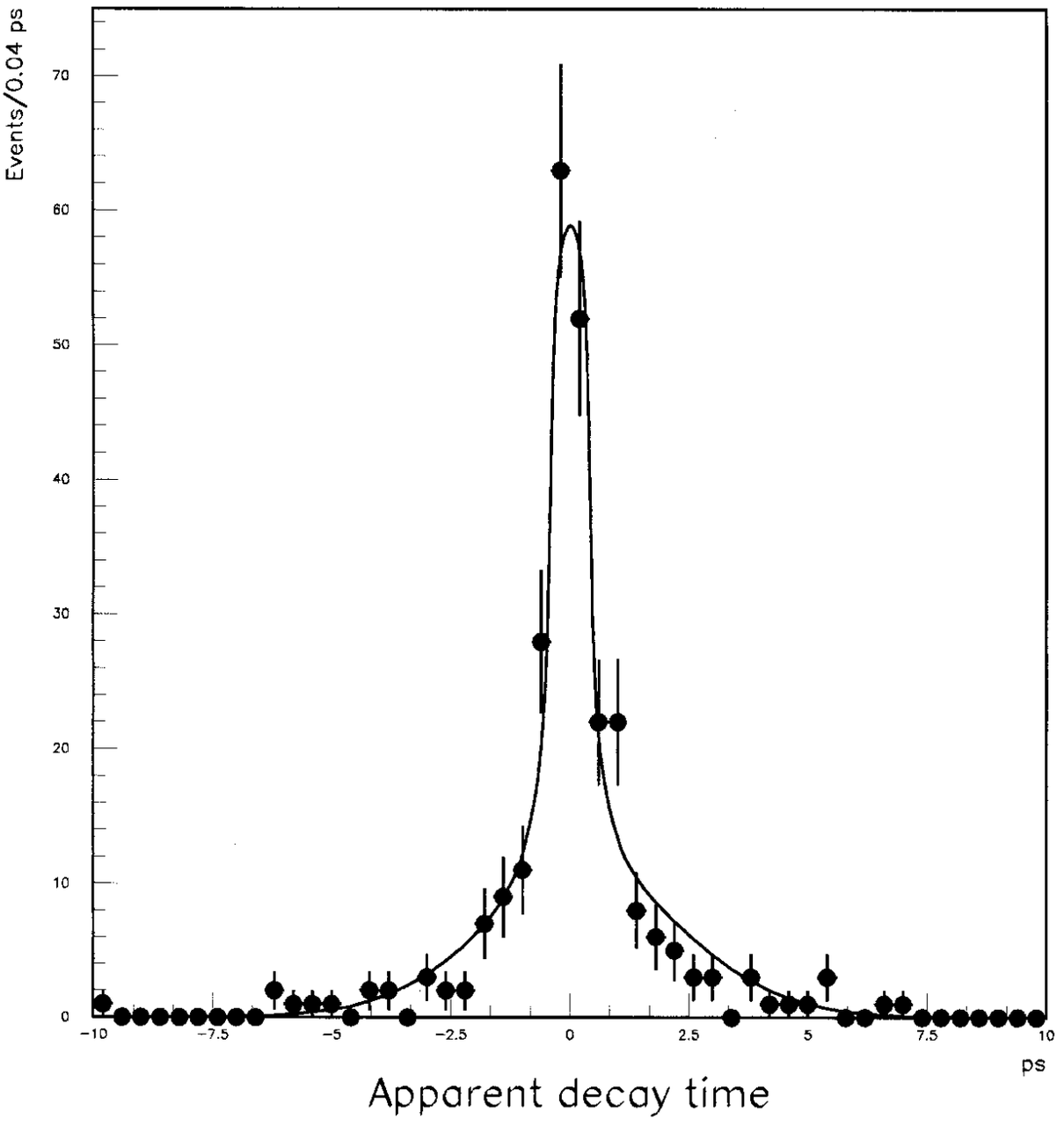

Figure 3: Apparent decay time distribution for the combined sample of events selected from outside the signal regions and from the $\overline{\mathrm{D}}^{(*)}\ell^-$ events. The solid line corresponds to the result of the maximum likelihood fit (see text).

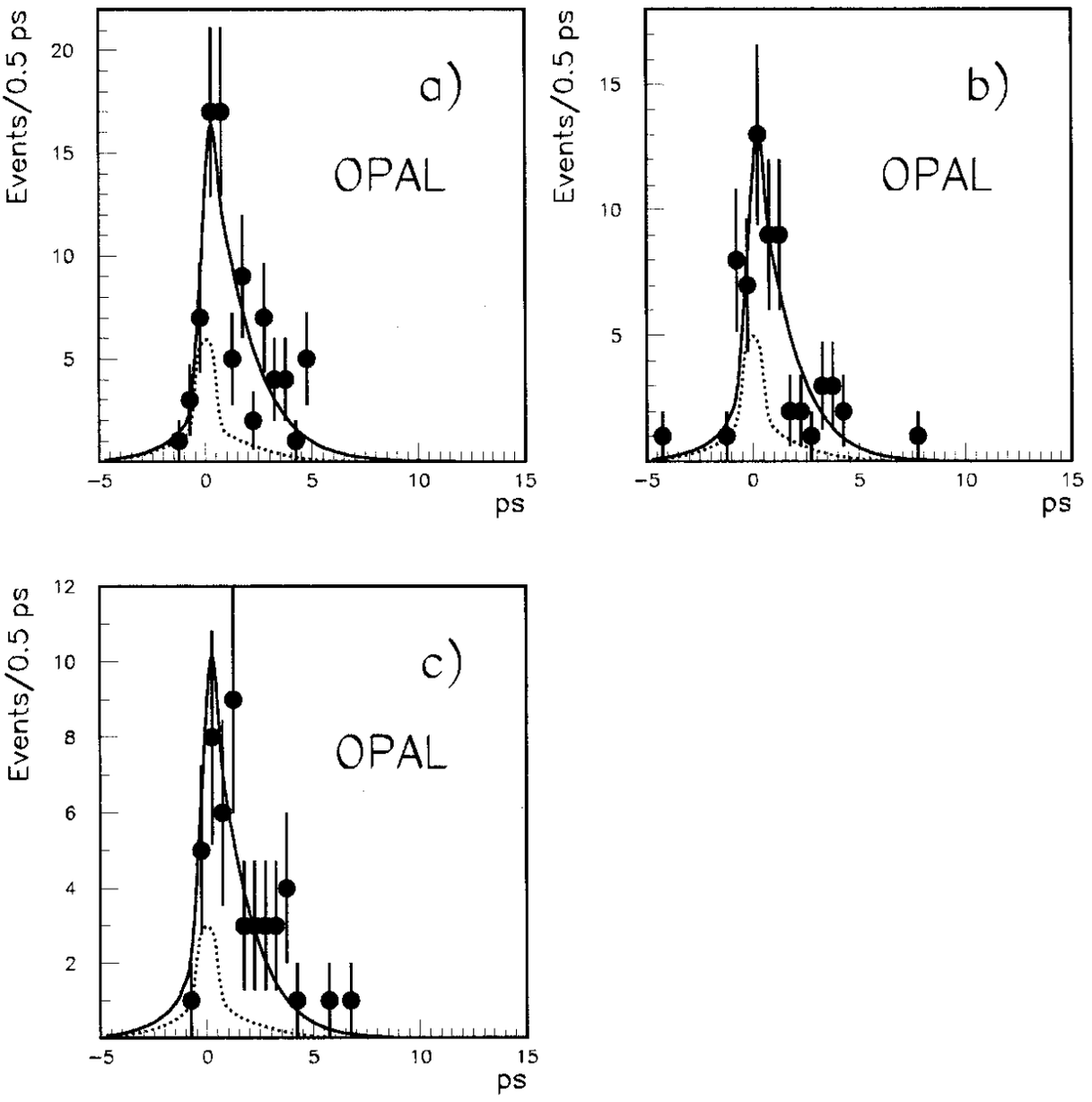

Figure 4: Decay time distributions for the different samples of $B \to \overline{D}^{(*)}\ell^+X$ candidates. (a) $\overline{D}^0\ell^+$ events, (b) $D^-\ell^+$ events, and (c) $D^{*-}\ell^+$ events. The solid lines are the results of the maximum likelihood fit. The dotted curves show the background contributions.

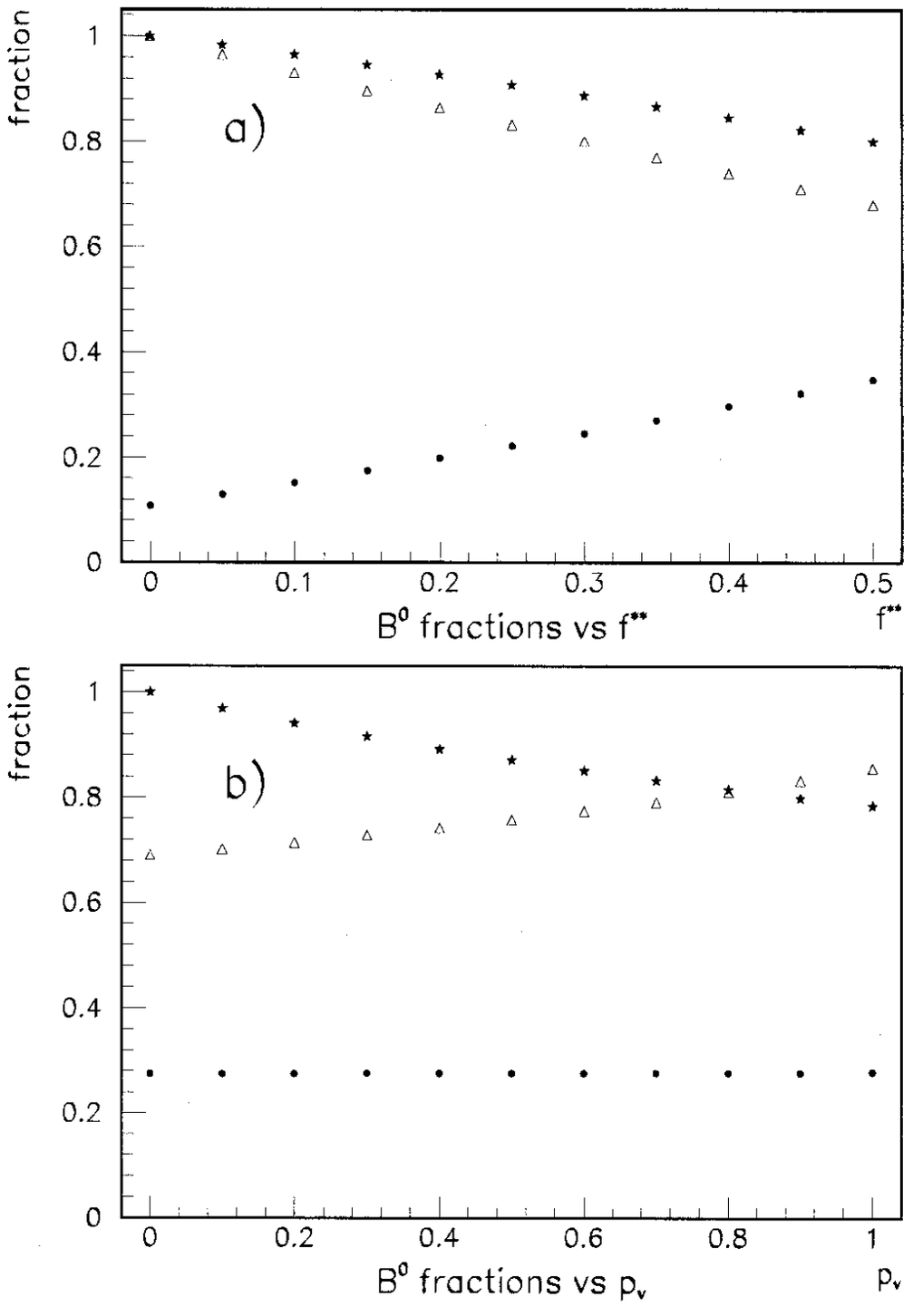

Figure 5: Predicted fraction of B^0 mesons in the samples of $\overline{D}^0\ell^+$ events ($\bullet$), $D^-\ell^+$ events ($\triangle$) and $D^{*-}\ell^+$ events ($\star$) as a function of (a) f^{**} with $p_v = 0.54$ and (b) p_v with $f^{**} = 0.36$.

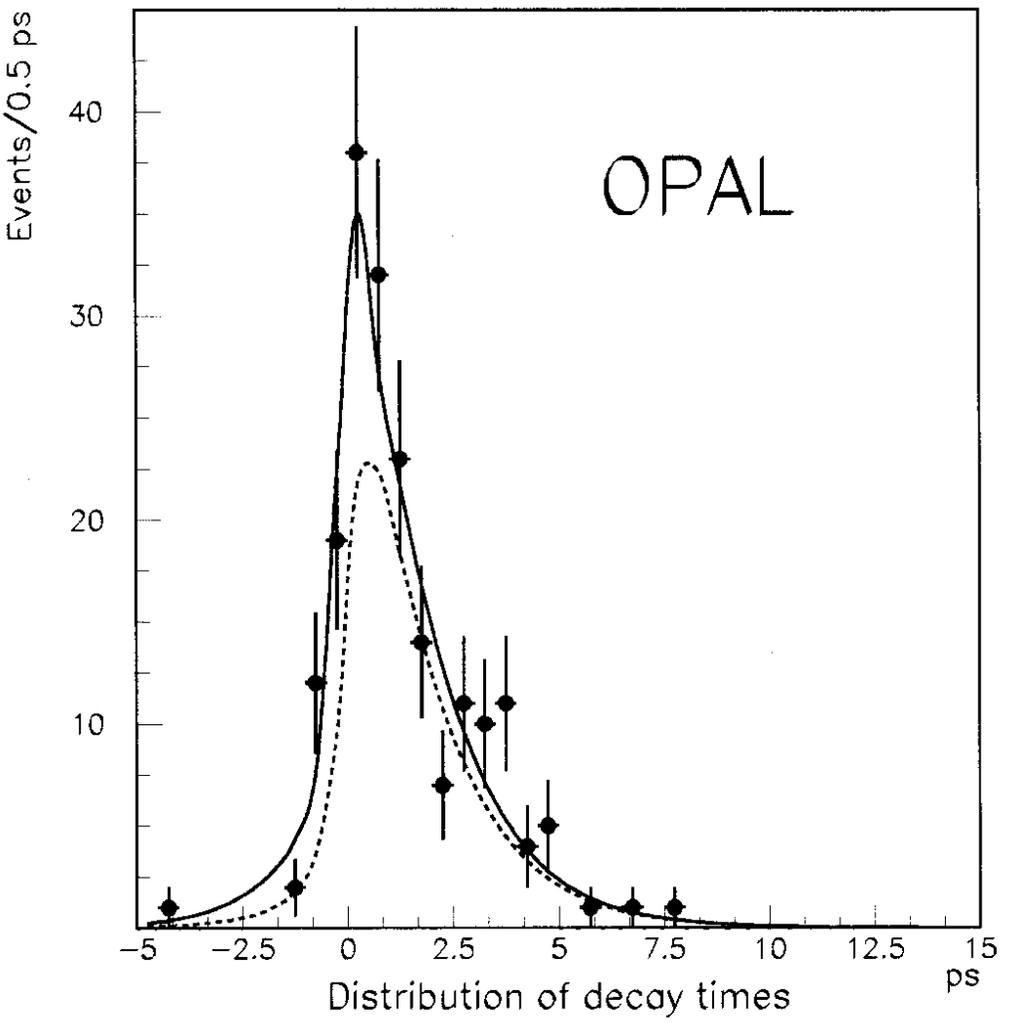

Figure 6: Reconstructed decay time distribution of the $B \to \overline{D}^{(*)}\ell^+X$ candidates. The solid curve is the result of the maximum likelihood fit. The dashed curve shows the sum of the fitted contributions from the B^0 and B^+ events.